Compliant Tactile Sensor Designed for Robotic Sensing Integration

James Tigue, Oleg Popkov, Ying Chen, Sandip Haldar, Hugh A. Bruck, Elisabeth Smela, Miao Yu

***Abstract*— Robots are currently designed to execute programmed actions to satisfy specific commands and motions. If a robot could be taught to do an action by a guiding touch from a human, rather than specific programmed actions, a single learning approach could be broadly applied to multiple robotic platforms. In order for a robot to learn from touch, the robot must have a sense of touch, the way a human does. To provide the robot with this sense of touch a novel sensing skin has been developed. This skin was created by applying a conductive exfoliated graphite/Latex mixture to a compliant Latex substrate. The skin is designed with a grid of strain gauges on both sides of the Latex substrate. Force, resistance, and strain characterization was conducted to determine skin performance. Responses from the skin have been seen to be time dependant under certain conditions. The skin has been shown to successfully localize external forces. Stain of the skin's surface has been shown to be directly related to skin response.**

Keywords—tactile sensor; strain gauge; compliant; robotic skin; exfoliated graphite;

I. Introduction

An effort to create a robotic skin has been conducted for over a decade. Efforts focused on the creation of a robotic tactile skin have been focused between resistive and capacitive devices [1-5]. Both of these types of methods generally guarantee low cost and power consumption, wide working ranges, and simple electronics. The implementation of capacitive sensing has advantages including temperature immunity and repeatable response. Capacitive devices, however, are largely vulnerable to large deformations that occur in a stretching environment. Because of this a focus on compliant resistive methods was chosen.

Resistive tactile sensors can be broken into two categories: piezoresitive and strain gauge. In general piezoresistors are made of semiconductor or metallic materials. Because of this material choice one of the major drawbacks to piezoresistive tactile sensors is their rigidity. To overcome this disadvantage, efforts have been made to combine peizoresistors with flexible polymers [1]. Many of these tactile sensors also are fabricated using MEMS techniques [4]. These techniques are time consuming and require diligent fabrication.

Strain gauge tactile sensors are based on the effect of geometry change on resistance. Normally strain gauges are made in long, thin, zig-zag patterns. These have been largely made with metallic or semiconductor materials. Again this creates a rigidity issue. To overcome this many authors have reported embedding of strain gauges in flexible substrates [1]. We will demonstrate that our process requires much less effort than a MEMS device and can withstand large deformations. Our proposed tactile sensor is a combination piezoresitive composite material used as a grid of strain gauges. Our chosen material is exfoliated graphite (EG) embedded in latex.

Only recently has EG been proven to be an effective component of compliant electrodes. Kujawski developed the manufacturing process for creating EG out of easily obtainable graphite [6]. He demonstrated the mechanical properties and uses of a compliant EG/PDMS mixture. Coupled with a polymer matrix, an effective EG piezoresistive strain gauge has been created and tested on a dynamic and static systems [7]. Wissman demonstrated the use of an EG/Latex strain gauge on the highly dynamic deformation of a MAV wing. These tests showed that an EG electrode is a relatively inexpensive alternative to other carbon based composite strain gauges.

In this paper we design a robotic skin made of a strain gauge grid using an EG and latex mixture. Characterizing the skin's response to forces and strains was preformed.

II. Methods

A. Sample Manufacturing

The strain gauges were made of a composite EG and latex (specs) mixture. Using the methods of preparation as in [7], an EG/water solution was created. This solution was then mixed with latex in a 25% wt mixture.

A sample of latex sheet was masked using blue painters tape (3M, 06818). On one side of the latex sheet eight vertical gauges were masked in a circular pattern (see Figure 1).

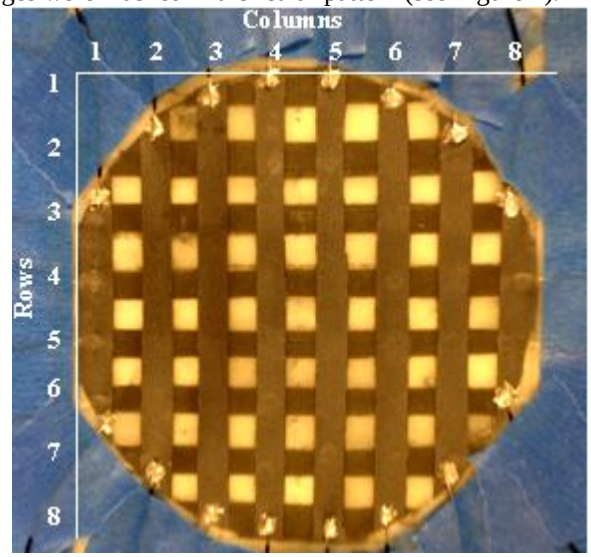

Figure 1. Strain gauge grid after final construction. Numbers indicate row and column reference numbers.

Funding Acknowledgment
NSF: REU Research Opportunities in Miniature Robotics
NRI: Small: Compliant Multifunctional Robotic Structures for Safety and Communication by Touch

On the other side 8 horizontal gauges were masked in a circular pattern. In this configuration, each gauge is isolated from the others. Each strain gauge was 0.5 cm wide. The diameter of the circle was 10 cm.

The uncovered areas were sprayed with the EG/Latex mixture to create a grid of strain gauges. Ten layers were sprayed. Each layer was allowed to dry for 10-20 minutes.

Wires were then attached to the ends of each strain gauge using small drops of two part silver conductive epoxy (MG Chemicals, 8331-14G). Blue painters tape was used to hold wires in place during setting time. Epoxy was allowed to set overnight.

Finally a foam substrate was used to support the skin. The skin was designed with foam to allow for large deformations of the surface and to act as the padding for the skin. The layering of the skin is shown in Figure 2.

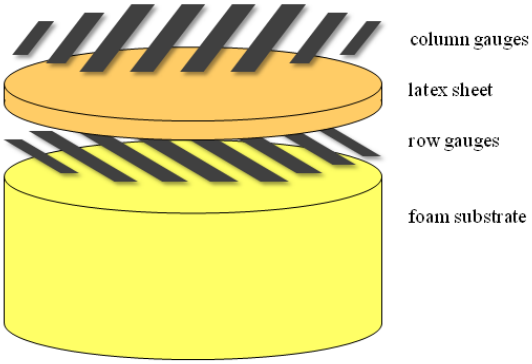

Figure 2. Diagram of layering of sensor.

B. Data Acquisition and Visualization

Each strain gauge in the grid was wired into identical circuits. Each gauge was powered with 5 VDC. In series with the gauge was a voltage divider resistor of 1000 ± 10 ohms. Voltage was measured across this voltage divider. A circuit diagram in Figure 3 depicts each gauge circuit.

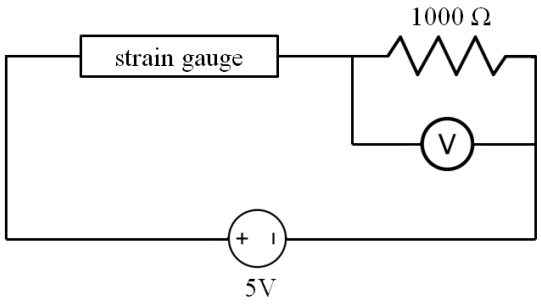

Figure 3. Circuit for each strain gauge in the grid. Each gauge is independent of the other gauges.

A Labview program (Grid_sensor_8x8_editted.vi) was created to collect voltage from each voltage divider and process it for visualization. The program first measures 200 samples of voltage from each of the 16 voltage dividers at 6000 Hz. These values are saved as a Labview measurement file (homo8x8.lvm). These initial voltages were used for comparison to all later measurements. This step was preformed once at the beginning of the program.

The program then begins a loop. Another set of voltages was measured and saved in a Labview measurement file (inhomo8x8.lvm). In each measurement file, time was also measured and saved.

The program runs Matlab script to process the voltage measurements. First the script averages both the 200 homogeneous voltages and the 200 inhomogeneous voltages. Then the voltages are converted into the resistance of the gauge using (1).

$$R_g = \left(\frac{V_s}{V} - 1\right) * R \tag{1}$$

R_g is the resistance of the gauge, V_s is the supply voltage 5 VDC, V is the average voltage drop across voltage divider, and R is the resistance of voltage divider. The homogenous resistances are saved as R_0 instead of R_g. The program then normalizes the inhomogeneous resistances with (2).

$$\frac{dR}{R} = \frac{R_g - R_0}{R_0} \tag{2}$$

A Matlab function (grid_recon.m) was written to take the 16 normalized resistances and return a 15 x 15 matrix of combined intersection resistances of the grid. The program separates the row and column normalized resistances and combines them at the intersections of row and column gauges using (3).

$$\Delta R(h, v) = \frac{dR}{R}(h) + \frac{dR}{R}(v) \tag{3}$$

$\Delta R_{(h,v)}$ is the combined resistance change that is stored in a 15 x 15 matrix. $\frac{dR}{R}(h)$ is the resistance of row gauge h and $\frac{dR}{R}(v)$ is the resistance of column gauge v. Since there are only 8 rows and 8 columns the remaining indices of the 15 x 15 matrix are linearly interpolated. The corners of the matrix were appropriately set to zero to be consistent with the circular shape.

This matrix was then plotted using the Matlab function colormap(). This creates a color map of the change in resistance across the entire surface of the strain gauge grid. See Figure 4 for a sample output from the full data acquisition and visualization program.

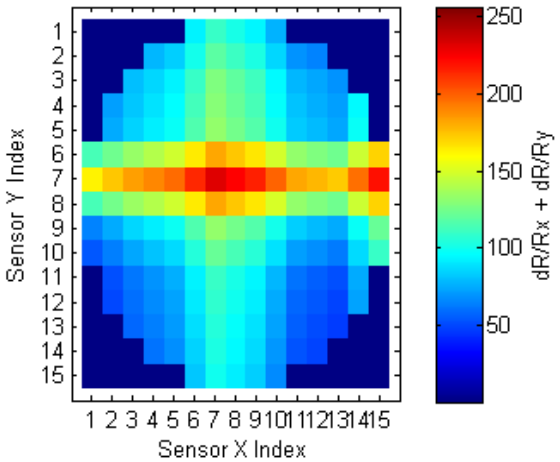

Figure 4. Example output of visualization program depicting a touch at row 4 and column 4. Color bar scale is percent change in hydrostatic resistance.

This visualization technique provides users visual feedback as well as a comparison for further characterization of the resistance and strain relationships. This plot is the final step for the program loop. The program starts over by measuring inhomogeneous voltages.

C. Force Testing

The goal of these tests was to develop an understanding of sensor response to forces applied perpendicular to the surface.

1) Set-up

Response from the tactile skin was tested using an Imada load frame (MX-500). A 2.5 kg max load cell was connected to the load frame probe. The tip of the load cell was covered with black electrical tape, to prevent unintentional grounding. A photo of the externally attached load cell can be seen in Figure 5.

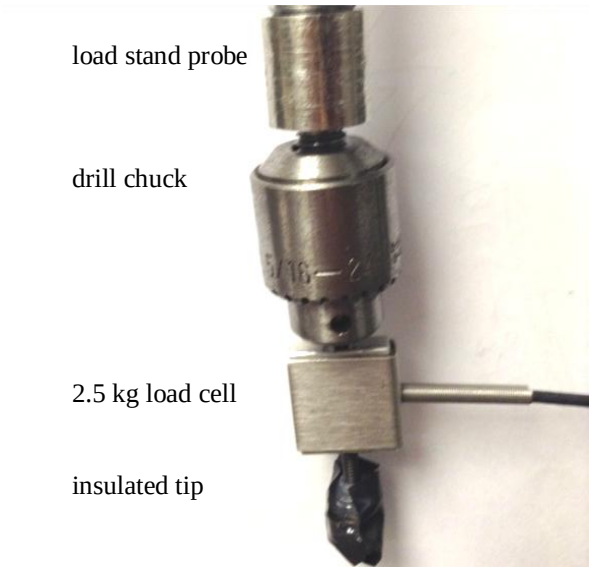

Figure 5. Photo of load frame probe connected to the external load cell.

By conducting a three point linear calibration with the load cell a relation between voltage and force was found. The sensitivity was 21.3 N/V. The bias was zero.

This load cell response was added to the Labview data acquisition program. The program was renamed (grid_sensor_8x8_with_force.vi). The program now saves force data at 200 samples at 6000 Hz in a Labview measurement file (Fdata.lvm). Further processing of this data would require an averaging of each 200 values per program loop.

A test fixture for the skin was also designed. The fixture kept the skin tight and stationary during testing. Two pieces of delrin plastic are clamped around the edges of the sensor and foam substrate.

After connecting the skin to the data acquisition circuit, the skin and fixture were placed on the load stand. A photo of the load stand force testing set-up can be seen in Figure 6 for a photo of the force testing set-up.

Figure 6. Photo of Imada load frame testing set-up.

The load stand operated by the user directing the probe up or down. The load stand held a constant position. The arrows on the interface control the direction and speed of the probe. The base speed was controlled by the dial. The single arrows move the probe at base speed and the double arrows move the probe at twice the base speed.

2) Measurements

Two tests were conducted using this testing platform. The first test was applying a deflection to the surface and holding that deflection. The goal of this test was to determine the response of the sensor in the event of a constant deflection. The probe was moved to provide an initial force of approximately 5 N. Force and sensor response were measured over 200 seconds of deflection.

The second test was applying a deflection and releasing the deflection and repeating. The goal of this test was to determine if the response of the sensor returned to the original value after deflection. The probe was moved to provide an initial force of approximately 5 N. Force and sensor response were measured over the 400 second duration of this test.

D. 3D Digital Image Correlation Experiments

Digital Image Correlation (DIC) is a full-field deformation measurement technique that has been applied to multiple length scales [8]. DIC was developed in the early 1980s [9]. DIC utilizes both optical imaging and numerical computing. DIC compares digitized images of an undeformed specimen to multiple images of deformed specimens. Gray scale speckle patterns are required for image reference during computation. The comparison of speckling in sequential imaging results in full-field deformation and strain.

3D DIC was developed in the 1990s [9]. 3D DIC employs two or more cameras to create a stereo vision system. 3D DIC is capable of calculation accurate surface deformations even under large three dimensional deformations.

1) Set-up

The 3D DIC measurement system was set up by using two cameras to take stereo images of a surface. The cameras (Point Grey, FL2G-13S2M-C) were used with specific lenses (Tokina, SD 12-24 F4 (IF) DX). The two cameras were placed as close as possible to each other, to create as similar images as possible. Additional lighting was added to the area of interest using (Lowel Pro, P2-10). The testing of the skin's surface and response took place on the Imada load frame. The set-up of camera and lighting for 3D DIC measurements are shown in Figure 7.

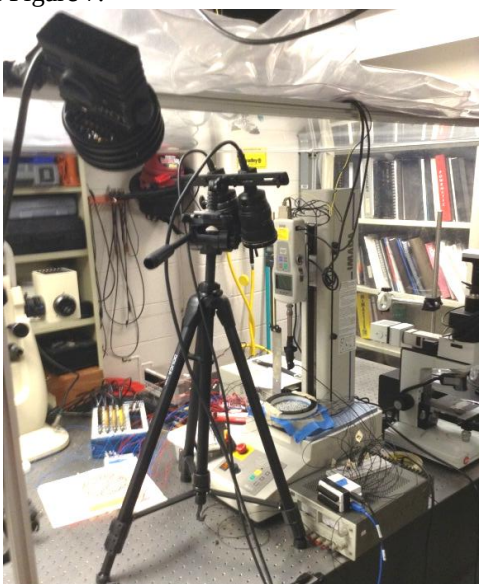

Figure 7. Photo of 3D DIC cameras and lighting set-up around Imada load frame.

The surface of interest needed to have high contrast speckling. To accomplish this, black latex paint (Behr, UL203) was applied to the skin's surface to create a uniform background and white dots of latex paint (Behr, UL200) were applied to create the speckling (see Figure 8).

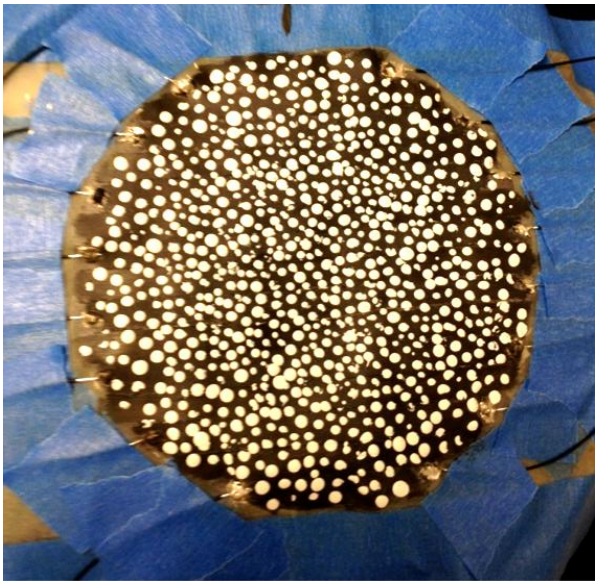

Figure 8. Photo of skin sample with final speckling.

This surface preparation allowed the processing software (VIC 3D 2010) to determine the shape of the surface. As the dots move in each picture the program determined the strain in the surface.

2) Calibration

In order for the software to correctly calculate the characteristics of the surface, a calibration was conducted. A calibration sheet was created from the program Dot Generator. The calibration sheet is a 16 x 16 grid with 6 mm spacing. The patter for calibration sheet can be seen in Figure 9 .

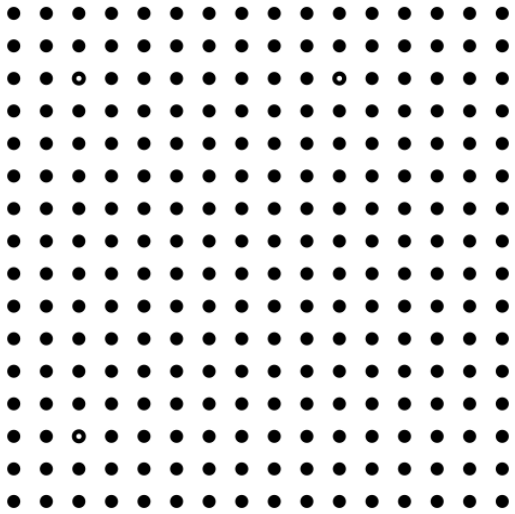

Figure 9. Pattern of calibration sheet. Each point is 6mm apart from others. The dots with white centers are the alignment dots.

The alignment dots were used by the program to orient the cameras. The locations of these dots were specified in the calibration.

Using this calibration sheet 2 photos were taken for each camera at 10 different positions. The images were simultaneously captured using the software VIC Snap 2009. These photos were then run through VIC 3D 2010 to calibrate the cameras. A calibration score of 0.118 was recorded.

3) Measurements

The Imada load frame was used to deflect the surface of the skin while the Labview program recorded data. The surface was deflected then unloaded. Images were taken during this process using VIC Snap. After the deflection was finished the images were processed by 3D DIC. The program generates 3D profile of the surface where different variables can be displayed in gradients on the surface. A sample surface can be seen in Figure 10.

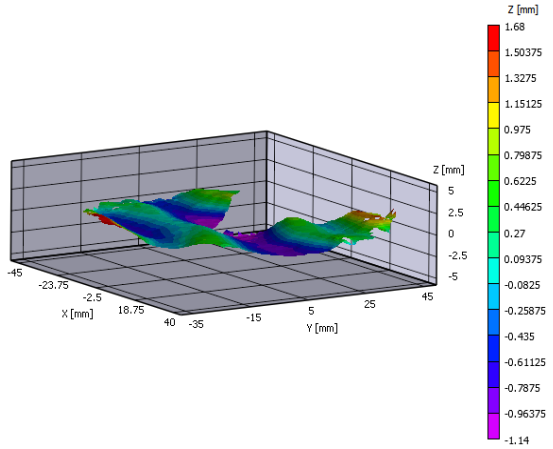

Figure 10. Example output of a 3D DIC analysis. This 3D contour plot can be configured for any variable of interest. In this image, the surface is not deflected by external forces.

All data calculated for this surface image was exported in a .csv file. Data from 3D DIC and responses from the skin were compared for strain and resistance relationships.

The area of the surface plot that is missing was caused by obstruction between the camera and the speckle surface. Figure 11 shows how the missing areas are caused by the load stand probe or lighting deficiencies.

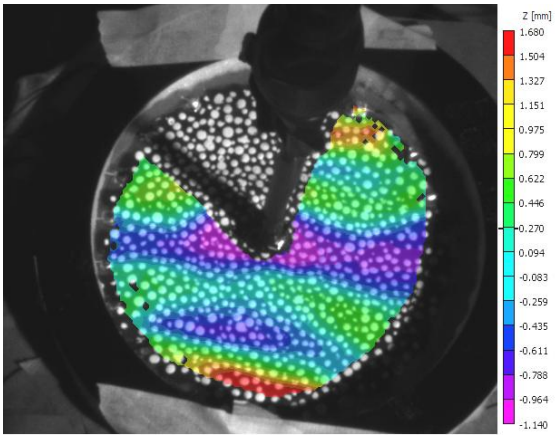

Figure 11. Example output of 3D DIC overlaid on surface image. This shows the missing areas of analysis caused by obstructions.

Areas with small holes in the surface reconstruction are caused by lighting insufficiencies. The large wedge of missing data was caused by the obstruction from the load stand probe and shadows.

III. Results and Discussion

A. Single Strain Gauge Characterization

1) Load Cycling

Using the force testing set-up, it was hypothesized that the gauges would not return to the original resistance after a deflection. To test this surface load was cycled. Figure 12 shows the response of the strain gauge during a load cycling.

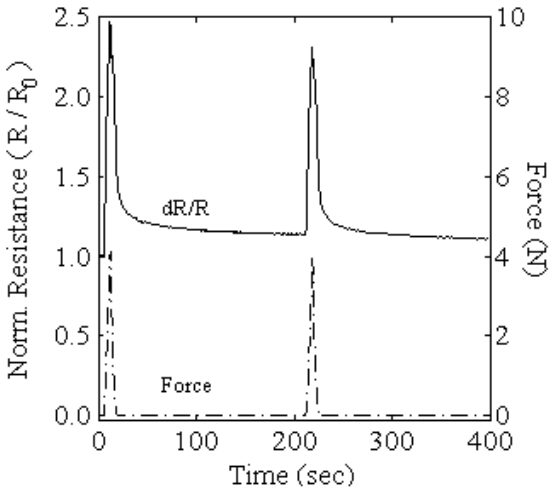

Figure 12. Plot of normalized resistance and force vs. time. This response is from one gauge while cycling a load with the force testing set-up.

When the load is applied to the surface the strain gauge responds immediately. On the first load cycle the resistance does not return to the original resistance. On the second load cycle the resistance returns to the value at the time of deflection. Each response has a degree of hysteresis as it settles to a value.

This response suggests that the strain gauge was physically changed upon the first deflection of the skin. This could be due to hysteresis effects of the EG/Latex solution. Further investigation into the behavior of the EG will provide an accurate characterization of this effect.

2) Constant Deflection

Because of time dependant behavior of the strain gauges during load cycling, it was hypothesized that the gauges would not hold a constant resistance under a constant deflection. Using the load stand, a constant deflection was applied to the surface. The responses from the strain gauge and the force applied were measured. Figure 13 shows the response of the strain gauge under constant deflection.

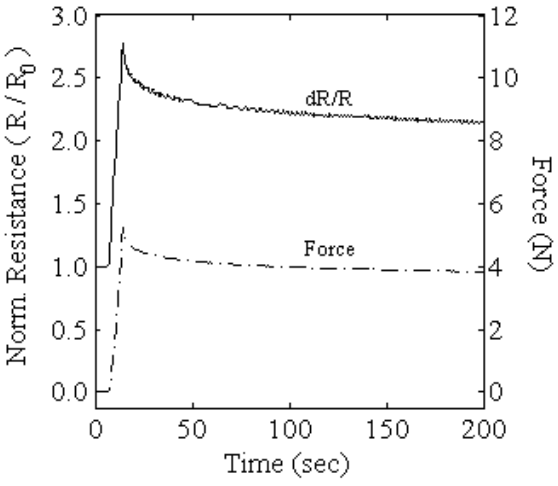

Figure 13. Plot of normalized resistance and force vs. time. This is the response of one gauge being deflected constantly over time.

In Figure 13, the normalized resistance of the strain gauge immediately responds to the applied deflection. At approximately 20 seconds the deflection is constant. Both normalized resistance and applied force begin to decay. The rate of decay decreases over the time scale. The rate of decay never reaches 0 over this time interval.

The decay of the resistance and the measured force were both similar. This response suggests that the stain gauge was relaxing or settling over time. Because both force and response decay at very similar rates, this response could be contributed to mechanical properties of both the latex sheet and the strain gauge.

Future test should be done over a longer time period. A larger time period could show if the strain gauge ever truly settles or not. Future test should also involve measuring the movement of the skin surface over time. This could be done using the 3D DIC analysis.

B. 3D Surface Measurements

From the 3D DIC setup, measurements of surface deflection during loading were conducted. The load was applied at the center of the skin gauge. This measurement was used to calculate strain and to compare to sensor response. The surface deflection can be seen in Figure 14.

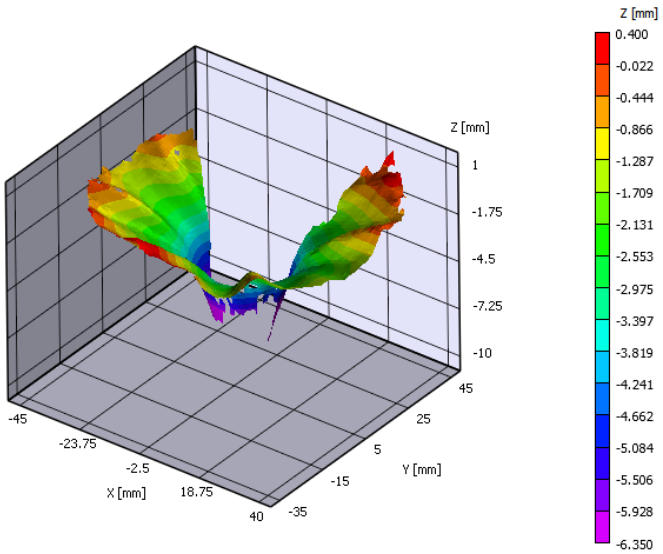

Figure 14. Contour plot of sensor surface. Grid scales indicate physical surface. Deflection is depicted with color gradient

This three dimensional representation of the skin surface shows non linear deflection across the radius of the circle. The surface has uniform deflection. This data will be used to calculate the strain of the surface.

When a material is under stress, the strain can be split into hydrostatic strain and deviatoric strain. Hydrostatic strain is the strain caused by squeezing. This is analogous to strain in a sphere balloon under water. Figure 15 shows hydrostatic strain of the sensor surface.

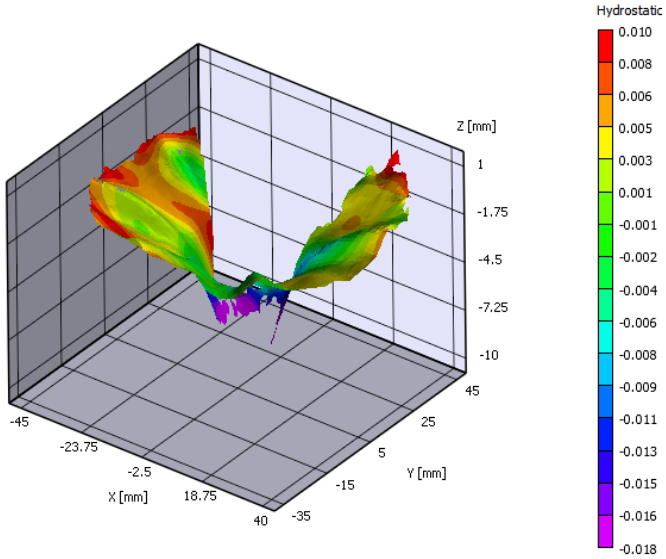

Figure 15. Contour plot of sensor surface. Grid scales indicate physical surface dimensions. Hydrostatic strain is depicted with color gradient.

Deviatoric is the strain that causes deflection in a material. Deviatoric is a strain tensor that can't be visualized with a single number for a finite point. To visualize the effective strain related to deflection a derived parameter of strain called Von Mises was calculated. This strain is used to compare to failure criterion of a material. Figure 16 shows the Von Mises strain of the skin surface during maximum load.

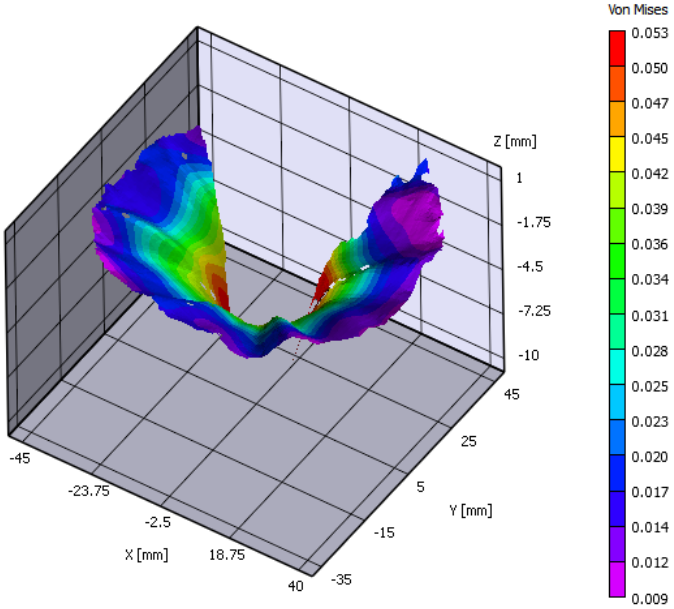

Figure 16. Contour plot of sensor surface. Grid scales indicate physical surface Von Mises strain is depicted with color gradient.

Strain depicted in Figure 16 decreases when approaching the boundary of the sensor. The strain is highest at the center and radiates outward. By comparing this strain and deflection to sensor response an understanding of the sensors capabilities can be established.

C. 3D Surface Characterization

The responses of multiple gauges are the first analyses of interest. For the skin to be an effective tactile sensor it should

localize an external force. By pressing at the center of the gauge, it was expected that the skin has a higher response at the center and decreasing responses away from the center. See Figure 17for the responses of column sensors.

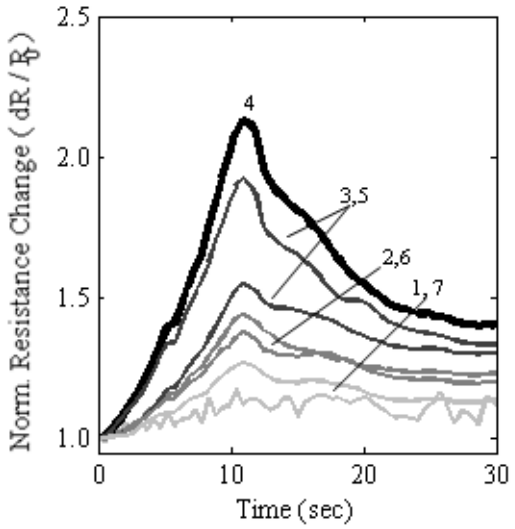

Figure 17. Plot of normalized resistance of individual column gauges when pressing on column 4. Grayscale depicts the decrease of distance from column 4 strain gauge.

As hypothesized the skin has a higher response at column gauge four. The gauge responses decrease as distance from the center increases. This confirms our expectations of force localization.

Using the 3D DIC and force testing set-up, measurements of sensor response and surface displacement were taken. The objective of these measurements was to characterize the response of the skin while under surface strain. Figure 18 displays the resulting shape of the surface during displacement.

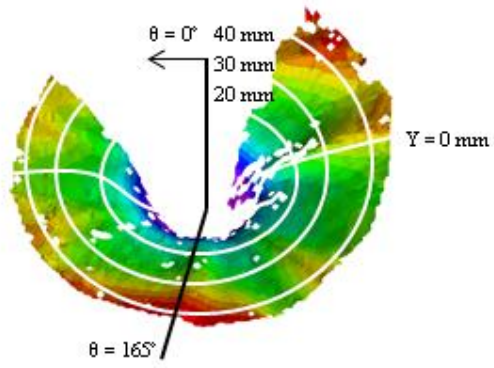

Figure 18. Diagram of data taken from 3D DIC analysis. Color gradient is Z deflection. White lines signify data sets of interest. These different data sets will be used in further analysis. At angle of 165 degrees is the peak of the rippling.

The black and white lines distinguish data sets of interest in further processing. Using these data sets a characterization of the skins response can be conducted. The color gradient indicates the Z displacement at maximum displacement.

The forces required to deflect the surface are of value. The evolution of shape of the skin sample on foam substrate is depicted in Figure 19.

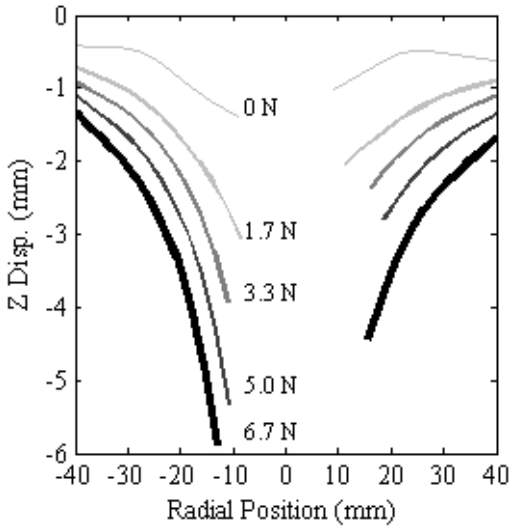

Figure 19. Deflection vs. radial position. Applied force is shown for each deflection. Data was taken along the horizontal line in Figure 18.

At 0 N the surface is not completely flat. As force increases the maximum deflection of the surface increases. Deflections increases uniformly. Data missing from the center of the plot is lost to obstructions in the 3D DIC imaging. This data shows that a correlation between surface strain and force could be made with further characterization.

Because this skin is not an idealized membrane, the skin seems to ripple when deflected. This ripple could contribute to noise, or error in localizing forces. In order to better under this surface condition analysis of the surface displacement was conducted (see Figure 20).

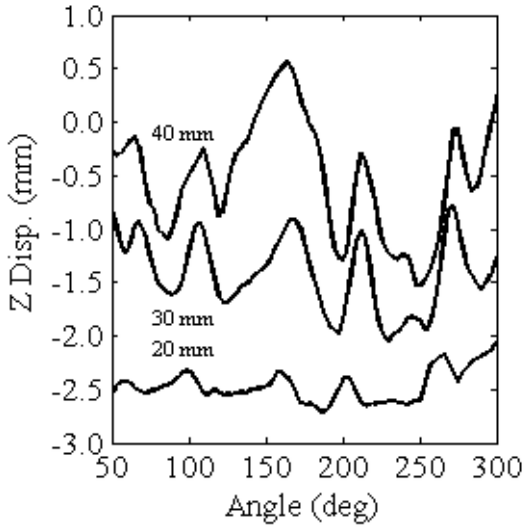

Figure 20. Plot of surface position vs. angle around center of surface. Labels indicate radius of circular data. (see Figure 18).

The rippling effect is largest further away from the center of impact. The pattern of this rippling is also consistent at

different between radii at different angles. Peak of rippling is at 165 degrees.

Gauge response is a function of stain in the gauge. To accurately characterize the response of the gauges, a connection to strain is analyzed. The shape of the deformation determines stain of individual gauges. Figure 16 explores the shape of the cross-section and the relationship between strain and gauge response.

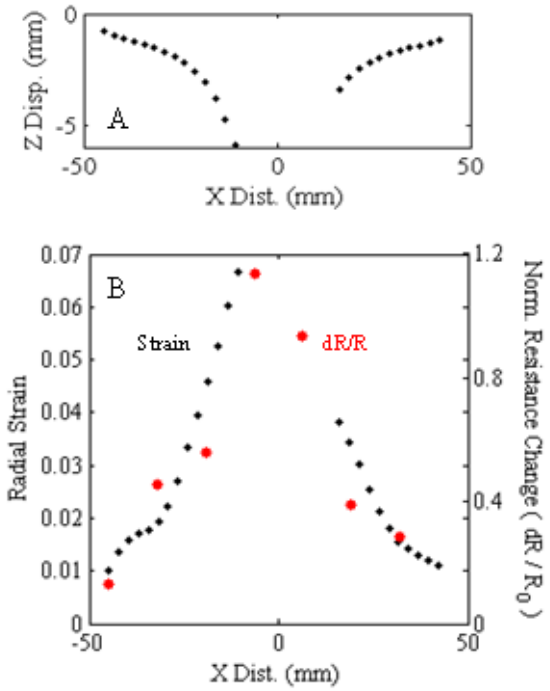

Figure 21. (A) Plot of displacement in the Z direction. This data is taken along the line (see Figure 18). (B) Radial strain (3D DIC) along radius of sensor is compared to the normalized resistance change of column gauges across sensor surface.

The cross-sectional view of the surface shows non-linear deformation. The deformation is also symmetric. Because strain is related to surface deformation, strain should also uniform.

In Figure 21 (B), strain and normalized resistance change follow the same curve. This result indicates that the response of the skin sensor is proportionally related to the strain. This figure validates the imaging capabilities of the skin sensor. Further investigation into response and strain measurement will able to provide response and strain correlations.

IV. Conclusions

The main purpose of the research was the development of a novel robotic skin. This skin was created with a compliant EG/latex strain gauge grid applied to a latex substrate. The skin is supported and protected by a foam layer. Figure 1 shows the final design of a circular skin sample.

A single gauge was tested for responses to applied forces. Tests revealed time dependant behaviors. The first time dependant behavior is tied to settling response after deflection of the skin. The second behavior is response decay under constant deflection. This behavior seems to be linked to physical changes in the strain gauge material. Further testing of this material will be able to elaborate on these time dependant responses.

Rippling was also discovered during 3D DIC testing. The rippling of the surface was shown to be larger at boundary conditions. At these locations strain is lowest. The rippling is very small in the areas of highest strain. Because of this characteristic rippling can be seen to have a small impact on the surface response.

A 3D characterization of the skin's response was conducted. The skin was shown to accurately localize applied forces in Figure 17. Using 3D DIC a strain analysis of the skin surface was conducted. As expected strain and skin response are directly related. The pattern of gauge response directly mimics the strain of the surface.

Further characterization of the skin's response to forces and strain must be conducted in order to fully understand the performance. With this information an application to a robotic platform could prove a concept of teaching robots by guidance.

Acknowledgments

This work was funded by the National Science Foundation (NSF) as a part of University of Maryland Miniature Robotics REU (award number 1062885). The work was also funded by NSF as a part of the project, NRI: Small: Compliant Multifunctional Robotic Structures for Safety and Communication by Touch (award number 1317913).

References

[1] S. Stassi et al, " Flexible Tactile Sensing Based on Piezoresistive Composites: A Review," Sensors , vol. 14, pp. 5296-5332, 2014.

[2] J. G. Alvite, "Robotic Skin," U.S. Patent 4694231 A, Sep 15, 1987.

[3] M. Y. Cheng, et al, "An Anthropomorphic Robotic Skin Using Highly Twistable Tactile Sensing Array," in 5th *IEEE Conference on Industrial Electronicsand Applications*, Taichung, 2010 , pp 650-655.

[4] Gábor Vásárhelyi, et al, " Tactile sensing arrays – design and processing,", vol. LXIII, pp. 22-27, 2008.

[5] Engel, Jonathan M., et al. "Multi-layer embedment of conductive and non-conductive PDMS for all-elastomer MEMS." *Hilton Head*. Vol. 6. 2006.

[6] M. Kujawski, et al, " Elastomers filled with exfoliated graphite as compliant electrodes," Carbon, vol. 48, pp. 2409-2417, 2010.

[7] J. Wissman, et al, " New compliant strain gauges for self-sensing dynamic deformation of flapping wings on miniature air vehicles," *Smart Material and Structures*, Vol. 22, no. 085031, 2013.

[8] S. Haldar, N. Gheewala, K. Grande-allen &, " Multi-scale Mechanical Characterization of Palmetto Wood using Digital Image Correlation to Develop a Template for Biologically-Inspired Polymer Composites," *Experimental Mechanics*, Vol. 51 , pp. 575–589, 2010.

[9] Sutton, M , et al, "The effect of out-of-plane motion on 2D and 3D digital image correlation measurements ," *Science Direct* , vol. 46 , no 10, pp.746 –757, 2008.